White-Light Nanosource with Directional Emission

Catherine Favre,[1] Véronique Boutou,[1] Steven C. Hill,[2] Wiebke Zimmer,[3] Marcel Krenz,[3] Hendrik Lambrecht,[1] Jin Yu,[1] Richard K. Chang,[4] Ludger Woeste,[3] and Jean-Pierre Wolf[1]

[1]*Laboratoire de Spectrométrie Ionique et Moléculaire (UMR5579), Université Lyon 1, 69622 Villeurbanne Cedex, France*
[2]*Army Research Laboratory, 2800 Powder Mill Road, Adelphi, Maryland 20783-1197*
[3]*Instiut fuer Experimentalphysik, Freie Universitaet Berlin, Arnimallee 14, 10195 Berlin, Germany*
[4]*Department of Applied Physics, Yale University, New Haven, Connecticut 06520-8284*

(Received 27 November 2001; published 26 June 2002)

We report the first observation of white-light emission from femtosecond laser-induced plasma in a water droplet. Such emission is not observed with water in a cell. The microdroplet acts as a lens, focusing the incident light to nanosized regions within itself and directing the emission from these regions primarily back toward the laser source. This focusing increases the intensity so that multiphoton ionization generates plasma and causes it to reach the critical density during the initial part of the pulse, enabling the rest of the pulse to heat the plasma enough to emit in the visible.

DOI: 10.1103/PhysRevLett.89.035002 PACS numbers: 52.50.Jm, 42.65.–k, 42.68.Jg

Nanosources, such as quantum dots or single molecules, are of interest in cavity QED and ultrahigh resolution microscopy [1]. The intensity of an incident wave at a nanosource, and the emission from a nanosource, can be enhanced when the source is within or on a microcavity, e.g., a spherical microresonator [2,3]. Nanosources emitting a broadband white-light (WL) spectrum in a preferential direction are of interest. Laser-induced nanosplasma has been observed in rare gas and metal clusters [4,5]. Laser-induced breakdown (LIB) involving multiionized ions and collective effects such as plasmon resonances could be a source for x-ray spectroscopy [6]. In these clusters the nanometric plasma size is due to the nanometric size of the particle itself.

We show here for the first time that (i) plasma-induced WL can be generated in water droplets excited with fs pulses (in contrast to fs illumination of water in a cell where no WL emission from plasma was detectable [7–9]), and (ii) the plasma generated in these droplets occurs in nanosized regions, i.e., the plasma in the droplet is a nanosource which is enclosed in a μm-sized droplet. Nanosized plasma can be produced within water droplets (50- to 70-μm diameter) because of internal focusing of the excitation intensity $I(\mathbf{r})$ ($\mathbf{r}$ is the position vector inside the droplet). Because the droplet acts as a spherical lens, and because the back surface acts as a spherical reflector, much of the incident light is focused to a small volume inside the droplet, where the intensity in a 50-μm-diameter water droplet may be enhanced 100 to 200 times the incident intensity I_i, in one or more closely spaced regions [Fig. 3(b) below]. Further localization is achieved for nonlinear excitation, which typically involves the nth power of the internal intensity $I^n(\mathbf{r})$. For WL plasma generation with 800 nm light, $n = 5$ photons [7,10] are required to ionize water. The high intensity in the focal volume allows multiphoton generated free electrons to build to the critical density during the initial part of the pulse and allows heating of these electrons during the remaining part of it. It is crucial to use fs excitation, to avoid significant expansion of the plasma, because the total laser energy deposited must be low. By comparing the measured angular distribution of the plasma emission with the calculated angular emission patterns (including emission calculated assuming the plasma source extends to a larger size than our analysis suggests it does), as well as by analyzing $I(\mathbf{r})$ and the plasma electronic density, we conclude that the plasma is localized to a nanometer-sized region. That the emitted light is strongly enhanced in the backward direction is relevant to applications such as remote analysis of aerosols and clouds (e.g., the return from a cloud should be highly sensitive to the droplet- or ice-crystal-size distribution). Light detection and ranging experiments, using ultrashort high intensity laser pulses, demonstrate that the required intensity for plasma generation can propagate over large distances [11]. The backward-enhanced plasma emission spectrum from water droplets or biological agents [12] could be attractive for remotely determining the composition of atmospheric aerosol.

In our experiment, the laser consists of a Kerr-lens mode-locked Ti:sapphire oscillator and a chirped-pulse amplifier, delivering 120 fs pulses at 810 nm at a 20 Hz repetition rate. The beam (a few μJ per pulse) incident on the droplets is approximated by a quasiplane wave because a long focal length lens (1 m) is used. The beam waist diameter, measured by diffraction on a fiber translated across the beam, is typically 5 times larger than the droplet diameter selectable between 50 and 70 μm). The water droplets are produced with a piezodriven nozzle source synchronized to the laser so that each pulse excites one droplet. The droplet size, shape, and position in the beam waist are monitored through a microscope and/or with forward scattering. The measured reproducibility is better than 5%.

The angular distribution of the far-field WL emission is measured between $\theta_d = 3°$ (near forward) and $\theta_d = 178°$

using a photomultiplier tube (PMT) mounted on a stepper-motor-driven goniometer (angular resolution = 2.2°). A green bandpass (500 ± 35 nm) filter in front of the PMT (with low quantum efficiency at 810 nm) blocks the 810 nm and the third-harmonic generation from the droplet [13]. The spectrum is measured at different angles with a low resolution spectrometer. To analyze the plasma lines, measurements in the backward direction are made with an intensified CCD camera. The polarization of the WL emission is analyzed near 180°.

Figures 1(a) and 1(b) show WL (500 ± 35 nm region) angular distributions at different incident intensities. At $I_i = 1.8 \times 10^{12}$ W/cm^2 [bottom of Fig. 1(a)], the emission is strongly enhanced in the backward direction, and has a narrow lobe near 150°. The luminance within the narrow lobe (±2° FWHM) at 180° is 7 mW · sr^{-1} · nm^{-1} while the intensity ratio $U_p(180°)/U_p(90°) > 35$. These features strongly suggest an extreme localization of the WL source (see below). When I_i is increased by 10× [Fig. 1(b)], the emission is brighter but more isotropic. The observed light is unpolarized [$U_{\text{perp}}(180°)/U_{\text{tot}}(180°) = 0.48$] at both I_i.

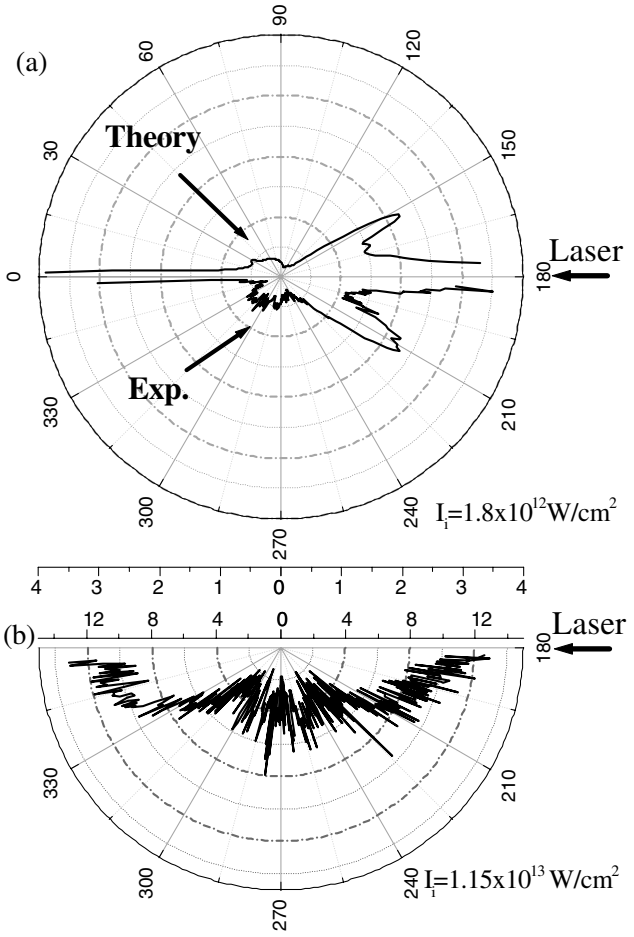

FIG. 1. (a) Comparison of the experimental and calculated angular distribution (AD) of WL emitted by a nanoplasma induced in a water microdroplet (diameter = 60 μm experimental, 22.6 μm calculated). (b) AD for higher experimental intensity.

The emission spectrum near 180° with $I_i = 5.2 \times 10^{12}$ W/cm^2 is shown in Fig. 2(a). Other processes, e.g., self-phase modulation (SPM) and sonoluminescence (SL), are able to generate WL in water, but only LIB can be the source of the emitted light in our case. Although SPM in a cell is efficient, especially in the fs regime where it can be enhanced by ionization [14], it does not explain our observations because (i) the interaction lengths in the highest intensity regions are too short to significantly broaden the initial bandwidth, (ii) for either I_i in Fig. 1, the emitted radiation is depolarized, which is characteristic of an incoherent process (not SPM), (iii) a simple ray-tracing analysis suggests that the SPM rays should be at rainbow angles (about 135°) rather than backwards (iv) the shape of the emitted spectrum [Fig. 2(a)] is consistent with a blackbody radiation process at a temperature about 7000 K, and (v) sodium D1-D2 lines in emission from water droplets containing NaCl [Fig. 2(b)] [still visible when I_i is decreased by 10× from that in Fig. 2(b)] strongly suggest laser-induced breakdown. Although laser-induced SL in water yields broadband optical emission [15], under our conditions it is unlikely to make a significant contribution because the WL emission is simultaneous (ns resolution) with the laser pulse, whereas the bubble collapse is delayed (μs time scale) [8].

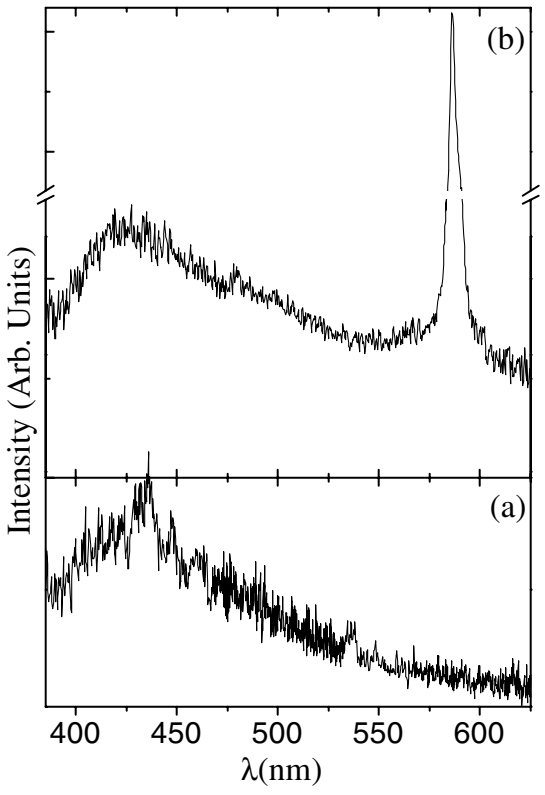

FIG. 2. Emitted WL spectrum from (a) pure water microdroplet, $I_i = 5.2 \times 10^{12}$ W/cm^2; (b) saline water microdroplet, $I_i = 1.9 \times 10^{13}$ W/cm^2. The maximum wavelength is not directly comparable because the MPI process (intensity and ionization potential dependent) for pure and saline water are different.

To understand why visible WL plasma emission is observed from droplets, but not in a cell, we calculated the plasma electronic density ρ by solving the rate equations [7,16] for multiphoton ionization (MPI), cascading, and losses by diffusion and recombination. The results, obtained using Runge-Kutta integration and the parameters of [7,16], are shown in Fig. 3(a) MPI (proportional to I^5) generates a steep rise of ρ during the leading part of the pulse. Cascading further increases ionization until the wavelength-dependent critical electronic density $\rho_{\text{crit}} = 1.7 \times 10^{21}$ cm^{-3} is reached [17]. At $\rho = \rho_{\text{crit}}$, the plasma becomes opaque and the remaining part of the laser pulse is absorbed by inverse bremsstrahlung, and the absorbed energy heats the plasma. As shown in Fig. 3(a), at 10^{12} W/cm^2, ρ_{crit} is never reached and the plasma remains transparent. At 10^{13} W/cm^2, less than 30% of the pulse energy is available to heat the plasma. In previous experiments in a cell, even though the maximum intensity level at the focus is about 10^{13} W/cm^2, the remaining portion of the laser pulse must heat a large plasma volume (typically 80 μm^3), and the energy density in the focal volume (typically 10^2 J $\cdot$ cm^{-3}) is low. Consequently, the plasma temperature in the cell is lower than that in a droplet, and the emitted spectrum is large in the infrared and undetectable in the visible [9].

A microdroplet is different because it focuses much of the incident light to one or more nanosized regions inside itself. The peak $I(\mathbf{r})$ may be 100 to 200 times I_i. Even at low I_i (e.g., 10^{12} W/cm^2), it reaches 10^{14} W/cm^2 [see Fig. 3(b)]. Then, the critical electron density ρ_{crit} can be reached during the beginning portion of the pulse [see Fig. 3(a)]. At $I(\mathbf{r}) = 10^{14}$ W/cm^2, the rate equations show that the plasma absorbs 95% of the pulse [Fig. 3(a)]. Neglecting scattering [18], the remaining energy (less than 0.4 nJ) is absorbed (until the energy density is 3×10^3 J $\cdot$ cm^{-3}), and the resulting high local temperature could bring the plasma emission into the visible. At the same I_i (10^{12} W/cm^2), the energy density in the focal volume of a cell is 10 times lower than it is in a droplet and hence the plasma in a cell doesn't reach ρ_{crit}.

We model the total radiation power $U_p(\theta_d)$ from the droplet, collected by a detector at angle θ_d (with respect to the incident beam) subtending a differential element of solid angle, $d\Omega$, as

$$U_p(\theta_d) = \int_V P(\mathbf{r}) F(\mathbf{r}, \theta_d)\, d\Omega/4\pi\, dV\,, \qquad (1)$$

where $P(\mathbf{r})$ is the WL emission power, $F(\mathbf{r}, \theta_d) d\Omega/4\pi$ is the probability that a photon emitted at $\mathbf{r}$ reaches the detection aperture, and V is the droplet volume. $P(\mathbf{r})$ is obtained from (i) the time-dependent electron density $\rho(\mathbf{r})$, calculated [7,16] as described in Fig. 3(a), and (ii) the time-integrated $I(\mathbf{r})$ [see Fig. 3(b)] obtained by integrating, over frequency (using Parseval's theorem), the intensity calculated using Mie theory (with more points near droplet resonances). $I(\mathbf{r})$ is assumed Gaussian in time [19] for obtaining $\rho(\mathbf{r})$. The absorption coefficient $\alpha(\mathbf{r})$ [7] is

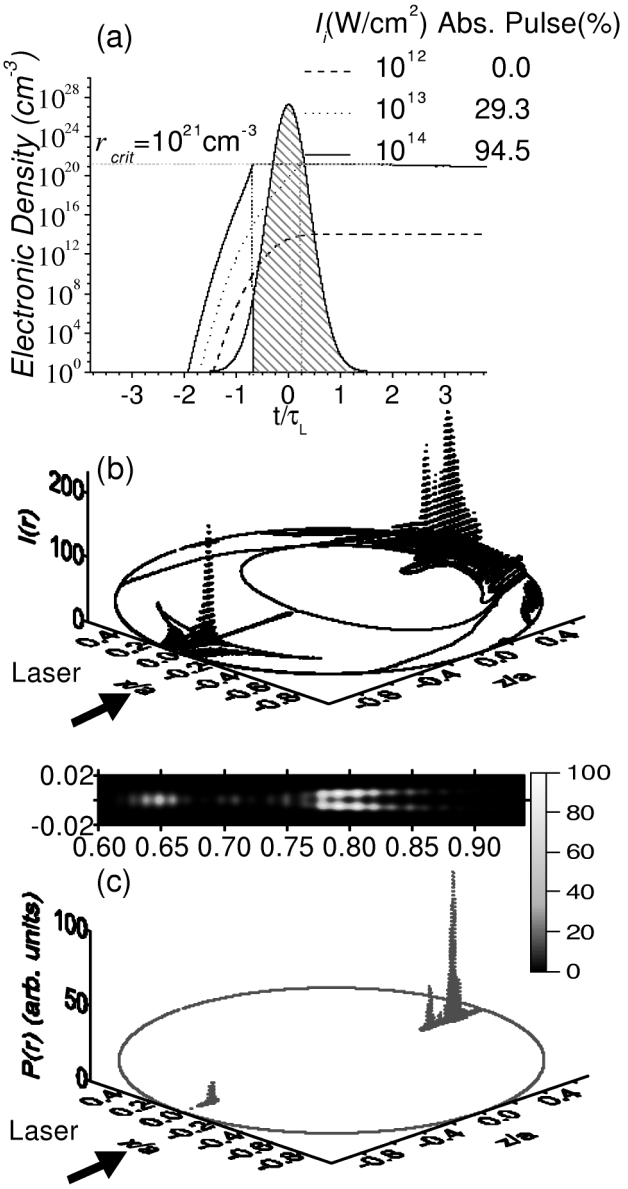

FIG. 3. (a) Electronic density evolution during the laser pulse duration ($\tau = 120$ fs, $\lambda = 810$ nm) for $I(\mathbf{r}) = 10^{12}$, 10^{13}, 10^{14} W/cm^2. (b) Calculated time-averaged intensity distribution $I(\mathbf{r})$ (relative to the intensity in free space) in a 60-μm-diameter water sphere ($m = 1.329 + i1 \times 10^{-6}$) illuminated with plane wave 120 fs (FWHM) Gaussian pulse with the electric field polarization vector in the x-z plane shown. The coordinates are normalized by droplet radius a. (c) Calculated distribution of $P(\mathbf{r})$ (in arbitrary units), the strength of the source of the WL emission inside the droplet in (b) when $I_i = 10^{12}$ W/cm^2. The inset shows the nanometric size of the main emitting plasma structures (0.03 μm^3 each).

calculated using $\rho(\mathbf{r})$ and $I(\mathbf{r})$. We assume that the absorbed energy density is $dE(\mathbf{r}) = I(\mathbf{r})\alpha(\mathbf{r})m\frac{dl}{c}$ (with dl a length unit) and that this energy increases the temperature by $dT(\mathbf{r})$ [9,20]. Because of the optical thickness in the plasma volume [$\alpha(\mathbf{r})dr = 2$], the WL emission power $P(\mathbf{r})$ is well approximated by the Stefan-Boltzmann law for blackbody radiation [proportional to $\sigma T^4(\mathbf{r})$, thus to $I^4(\mathbf{r})\alpha^4(\mathbf{r})$ [18]]. Figure 3(c) shows the calculated

$P(\mathbf{r})$ distribution in the equatorial plane of the droplet. The higher resolution inset shows the emitting plasma region, which consists of several nanosized regions, each with a typical volume of 0.03 μm^3. These regions result from constructive interference, are separated from each other by about $\lambda/(2m)$, and, because the incident field is polarized, are not axisymmetric. In calculating $F(\mathbf{r}, \theta_d)$, the fields from isotropic sources are expanded in spherical harmonics and matched at the surface of the sphere. $F(\mathbf{r}, \theta_d)$ is integrated over the broadband detected spectrum [21], and has a spatial distribution similar to that of $I(\mathbf{r})$ [21]. In calculating $I(\mathbf{r})$ and $F(\mathbf{r}, \theta_d)$ we assume that the plasma density is low enough that the droplet is homogeneous. The angular distribution of the emitted light is a 3D convolution of $P(\mathbf{r})$ and $F(\mathbf{r}, \theta_d)$, and is sensitive to the shape of each. The far-field emission $U_p(\theta_d)$ simulated for 22.6 μm diameter spheres is compared to measurements in Fig. 1(a). We cannot at present calculate for larger spheres because of CPU time and memory limitations [Eq. (1) requires integration over droplet volume], but calculations of $U_p(\theta_d)$ for other droplet sizes show no significant difference for diameters larger than 16 μm.

The remarkable agreement in Fig. 1(a) is consistent with the emitting plasma region being confined to a nanosized volume and, thereby, acting as a WL nanosource. The angular distribution and, in particular, the 150° peak and the backward enhancement are sensitive to the size of the emitting volume. Both quantities decrease as the emitters extend beyond the original nanoplasma region [Fig. 3(c)]. We therefore believe that the expansion of the radiating plasma is not significant. The weak plasma expansion is also consistent with the low total energy (0.4 nJ) imparted into the plasma even though it energy *density* is high enough to generate radiation in the visible. At higher I_i [1.1×10^{13} W/cm^2, instead of 1.8×10^{12} W/cm^2 shown in Fig. 1(a)], the observed angular distribution of Fig. 1(b) is more isotropic, consistent with the remaining part of the pulse heating the initially nanosized plasma, and inducing plasma expansion (as in the case of ns excitation, [22,23]). Moreover, the regions where the intensity approaches 10^{14} W/cm^2 spread into different parts of the droplet (also on the droplet front side) resulting in a change of the emission distribution.

We also measured the broadband visible emission from saline droplets with various I_i. When I_i is increased by 10× from 10^{12} W/cm^2, the emission spectrum shifts towards the blue (the maximum is shifted from 600 to 400 nm), consistent with an increase of the plasma temperature from $T(K) = 5000$ to 7000 K. The plasma temperature estimated is an average value because the emitted radiation is a sum of Planckians.

In summary, within water microdroplets, the tight focusing and the nonlinearity of the LIB process generate a nanosized plasma hot enough to emit in the visible, and preferentially in the backward direction.

R. K. C. and J. P. W. acknowledge NATO's support (Grant No. SST CLG 977928). J. P. W. also acknowledges the Institut Universitaire de France.

[1] J. Michaelis, C. Hettich, J. Mlynek, and V. Sandoghdar, Nature (London) **405**, 325 (2000).
[2] N. Lermer, M. D. Barnes, C-Y. Kung, W. B. Whitten, and J. M. Ramsey, Opt. Lett. **23**, 951 (1998).
[3] X. D. Fan, M. C. Lonergan, Y. Z. Zhang, and H. L. Wang, Phys. Rev. B **64**, 115310 (2001).
[4] T. Ditmire, T. Donnelly, A. M. Rubenchik, R. W. Falcone, and M. D. Perry, Phys. Rev. A **53**, 3379 (1996).
[5] T. Döppner, S. Teuber, M. Schumacher, J. Tiggesbäumker, and K. H. Meiwest-Broer, Appl. Phys. B **71**, 357 (2000).
[6] S. Dobosz, M. Schmidt, M. Perdix, P. Meynadier, O. Gobert, D. Normand, K. Ellert, T. Blenski, A. Y. Faenov, A. I. Magunov, T. A. Pikuz, I Y. Skobelev, and N. E. Andrew, J. Exp. Theor. Phys. **88**, 1122 (1999).
[7] J. Noack and A. Vogel, IEEE J. Quantum Electron. **35**, 1156 (1999).
[8] E. Abraham, K. Minoshima, and H. Matsumoto, Opt. Commun. **176**, 441 (2000).
[9] P. K. Kennedy, D. X. Hammer, and B. A. Rockwell, Prog. Quantum Electron. **21**, 155 (1997).
[10] F. William, D. P. Varma, and S. Hillenius, J. Chem. Phys. **64**, 1549 (1976).
[11] P. Rairoux, H. Schillinger, S. Niedermeier, M. Rodriguez, F. Ronneberger, R. Sauerbrey, B. Stein, D. Waite, C. Wedekind, H. Wille, L. Wöste, and C. Ziener, Appl. Phys. B **71**, 573 (2000).
[12] Y-L. Pan, S. C. Hill, J. P. Wolf, S. Holler, R. K. Chang, and J. R. Bottiger, Appl. Opt. **41**, 2994 (2002).
[13] J. Kasparian, B. Krämmer, J. P. Dewitz, S. Vadja, P. Rairoux, B. Vezin, V. Boutou, T. Leisner, W. Hübner, J. P. Wolf, l. Wöste, and K. H. Bennemann, Phys. Rev. Lett. **78**, 2952 (1997).
[14] A. Brodeur and S. L. Chin, J. Opt. Soc. Am. B **16**, 637 (1999).
[15] O. Baghdassarian, H.-C. Chu, B. Tabbert, and G. A. Williams, Phys. Rev. Lett. **86**, 4934 (2001).
[16] P. K. Kennedy, IEEE J. Quantum Electron. **31**, 2241 (1995).
[17] W. Theobald, R. Hassner, R. Kingham, R. Sauerbrey, R. Fehr, D. O. Gericke, M. Schlanges, W-D. Kraeft, and K. Ishikawa, Phys. Rev. E **59**, 3544 (1999).
[18] A. Vogel, J. Noack, K. Nahen, D. Theisen, S. Busch, U. Parlitz, D. X. Hammer, G. D. Noojin, B. A. Rockwell, and R. Birngruber, Appl. Phys. B **68**, 271 (1999).
[19] L. Mees, G. Gouesbet, and G. Grehan, Opt. Commun. **199**, 33 (2001).
[20] D. Arnold and E. Cartier, Phys. Rev. B **46**, 15 102 (1992).
[21] S. C. Hill, V. Boutou, J. Yu, S. Ramstein, J. P. Wolf, Y-l. Pan, S. Holler, and R. K. Chang, Phys. Rev. Lett. **85**, 54 (2000).
[22] J. H. Eickmans, W.-F. Hsieh, and R. K. Chang, Opt. Lett. **12**, 22 (1987).
[23] J-Z. Zhang, J. K. Lam, C. F. Wood, B. T. Chu, and R. K. Chang, Appl. Opt. **27**, 4731 (1987).